Resonances of $CH_2(\tilde{a}\,^1A_1)$ and their roles in unimolecular and bimolecular reactions

Shi Ying Lin and Hua Guo
Department of Chemistry, University of New Mexico, Albuquerque, New Mexico 87131

Stavros C. Farantos
Department of Chemistry, University of Crete and Institute of Electronic Structure and Laser, Foundation for Research and Technology—Hellas, Iraklion 71110, Crete, Greece

(Received 30 November 2004; accepted 12 January 2005; published online 29 March 2005)

Low-lying resonances of the $CH_2(\tilde{a}\,^1A_1)$ system ($J=0$) in an accurate *ab initio* potential energy surface are studied using a filter-diagonalization method. The width of these resonances fluctuates by more than two orders of magnitude and on average increases with the energy. Analysis of the resonance states concludes that the unimolecular decay of the excited molecular system near the dissociation threshold is neither mode specific nor statistical state specific. This is apparently due to remnant regularity embedded in the largely chaotic classical phase space, as evidenced by periodic orbit analysis. As a result, the Rice–Ramsperger–Kassel–Marcus and statistical adiabatic channel models overestimate the average unimolecular decay rate. The implications of the resonances for the bimolecular $C(^1D)+H_2$ reaction are also discussed. © *2005 American Institute of Physics*.
[DOI: 10.1063/1.1866094]

I. INTRODUCTION

Recently, there is much interest in the $C(^1D)+H_2 \rightarrow CH+H$ reaction mainly due to two reasons. From a practical perspective, this reaction is believed to play an important role in many chemical processes, such as combustion[1] and astrochemistry.[2] A perhaps more fundamental motivation stems from its uniqueness in understanding insertion reactions, which are often characterized by low or zero entrance/exit channel barriers and long-lived complexes.[3,4] Indeed, the reaction is almost thermoneutral and is dominated by a deep ($\sim$4.3 eV) CH_2 potential well.[5] Unlike the extensively studied $O(^1D)+H_2$ reaction in which nonadiabatic abstraction pathways may be involved,[6–8] the $C(^1D)+H_2$ reaction is believed to proceed via an exclusively adiabatic insertion pathway,[9] thus serving as an ideal prototype for understanding the dynamics of such reactions.

Despite the accumulation of experimental data on this reaction,[10–16] it is only recently that quantum mechanical studies of the reaction dynamics have been carried out[5,17–24] on accurate global potential energy surfaces (PESs) based on high quality *ab initio* calculations with large basis sets and inclusion of electron correlations.[5,25] In addition to confirming the barrierless insertion pathway,[26,27] these quantum studies have shown that the reaction probability is highly oscillatory, which has been attributed to the involvement of resonance states. Interestingly, the long lifetime of these resonances allows a statistical treatment of the reaction, which has been shown to be very successful.[21–24] Until now, however, no detailed study of these resonances has been attempted. Obviously, a better understanding of these metastable states, a major goal of this work, is of crucial importance for validating the statistical treatment of the bimolecular reaction and for gaining deeper insight into the reaction dynamics.

The deep CH_2 potential well supports a large number of bound vibrational states. There have been extensive spectroscopic studies of the rovibrational spectra of both the singlet and triplet manifolds of CH_2.[28–30] To our best knowledge, there has been no report of unimolecular dissociation of the molecule, but it is certainly not out of the reach of modern spectroscopic methods such as overtone pumping and stimulated emission pumping. Very recently, highly excited vibrational levels up to the dissociation limit of the lowest adiabatic singlet ($a\,^1A_1$) state have been reported by us.[31] It was found that the vibrational dynamics is largely chaotic, rendering many highly excited vibrational states irregular and unassignable. However, embedded in the chaotic spectrum there also exist regular states that defy the strong mode mixing. These behaviors of the highly excited bound states are expected to continue into the continuum, as shown in this work.

Many of the metastable resonance states apparently participate in the bimolecular reaction between $C(^1D)$ and H_2, as inferred from the oscillatory structure in the reaction probability. Due to the small exothermicity of the reaction, these resonance states are expected to be long lived, as evidenced by the sharpness of the oscillation. Consequently, the calculation of these states represents a computational challenge because of the large grid/basis size and long wave packet propagation necessary to converge them. This is particularly true if a Fourier based spectral method is used, because the resolution of a dense spectrum is dictated by the uncertainty principle. In this work, we employed a Chebyshev-based filter-diagonalization method to map out the complex energies of low-lying resonance states ($J=0$) with even exchange symmetry. In order to understand the corresponding classical

phase space, periodic orbit analyses were carried out. The distribution of the decay rates of the resonance states was compared with the Rice–Ramsperger–Kassel–Marcus (RRKM) and statistical adiabatic channel models[32] to shed light on the mechanism of the unimolecular reaction. In addition, their role in the bimolecular reaction was also explored. This paper is organized as follows. In Sec. II, the computational methods used in this work are briefly outlined. The results are presented and discussed in Sec. III. Finally conclusions are made in Sec. IV.

II. THEORY

A. Resonance calculations

The nonrotational ($J=0$) Hamiltonian used to calculate the resonance states is given in the reactant Jacobi coordinates,

$$\hat{H} = -\frac{1}{2\mu_R}\frac{\partial^2}{\partial R^2} - \frac{1}{2\mu_r}\frac{\partial^2}{\partial r^2} + \left(\frac{1}{2\mu_R R^2} + \frac{1}{2\mu_r r^2}\right)\hat{j}^2 + V(R,r,\gamma), \tag{1}$$

where r and R are, respectively, the diatomic (H−H) and atom-diatom (C−H_2) distances with μ_r and μ_R as their reduced masses. $\hat{j}$ denotes the diatomic rotational angular momentum operator. Reactant Jacobi coordinates (R,r,γ) were employed to make use of permutation symmetry. The PES used in this work is that of Banares *et al.*,[25] which was modified from the original *ab initio* PES of Bussery-Honvault, Honvault, and Launay.[5]

The resonances of interest are quasibound states embedded in the continuum above the scattering asymptote.[33] These so-called Feshbach resonances are formed because of temporary trapping of energy in some internal degrees of freedom. Although sharing some spatial features with bound states, they are fundamentally different in their boundary conditions. Indeed, the resonance states can be conveniently considered as eigenstates of a modified Hamiltonian made up of the original Hermitian Hamiltonian and a complex optical potential in the dissociation asymptotes.[34] The optical potential imposes outgoing wave boundary conditions[35] and permits the use of square-integrable bases. The corresponding eigenvalues are thus complex and in the form $E_n - i\Gamma_n/2$ where E_n and Γ_n represent positions and widths of the resonances, respectively. The resonance lifetimes, which are related to the widths $1/\Gamma_n$, are associated with the unimolecular reaction rates in the nonoverlapping resonance limit.[32]

To avoid the steep scaling laws in direct diagonalization, we employed the filter-diagonalization (FD) method originally introduced by Neuhauser,[36] which uses filter operators to generate a small subspace spanned by filtered states near the energy of interest, from which the approximate eigenvalues and eigenstates can be obtained. The filtering can be carried out with time propagation, but propagation based on polynomial recursion relationships[37–42] is preferred because they can be implemented exactly.[43] FD was further developed to avoid the explicit construction of the filtered states.[44] The so-called low-storage FD (LSFD) constructs small energy–local Hamiltonian matrices from correlation functions, preferably obtained from the Chebyshev propagation.[45–47] This approach is applicable to both real and complex symmetric Hamiltonians.[48–50]

Recently, we suggested an empirical scheme to double the Chebyshev autocorrelation function, $C_k \equiv (\psi_i|T_k|\psi_i)$, where T_k is the Chebyshev propagator.[51,52] It allows a more efficient determination of positions and widths of narrow resonances using LSFD. (A similar scheme was suggested later by Neumaier and Mandelshtam.[53]) The doubling scheme was used here to extract the resonance energies and widths of CH_2. To this end, the doubled autocorrelation function was calculated as follows:

$$C_{2k} = 2(\psi_k|\psi_k) - C_0, \quad C_{2k+1} = 2(\psi_{k+1}|\psi_k) - C_1, \tag{2}$$

where $(\bullet|\bullet)$ defines complex nonconjugate inner product,[54] and $\psi_k \equiv T_k\psi_i$.

The damped propagation in the Chebyshev order domain was performed to enforce outgoing wave boundary conditions,[39,40]

$$\psi_{k+1} = D[2\mathbf{H}_{norm}\psi_k - D\psi_{k-1}], \tag{3}$$

with $\psi_1 = D\mathbf{H}_{norm}\psi_i$. The Hamiltonian was normalized, $\mathbf{H}_{norm} = (\mathbf{H} - H_+)/H_-$, so that $H_{norm} \in [-1,1]$, where $H_\pm = (H_{\max} \pm H_{\min})/2$ and $H_{\max}(H_{\min})$ is the upper (lower) bound of the spectrum.[55] The damping function D is arbitrary as long as it smoothly decays at the grid edges. In this work, we used the following form:

$$D(R) = \begin{cases} 1 & \text{for } R \leqslant R_d \\ e^{-d_R(R-R_d)^2} & \text{for } R > R_d \end{cases}. \tag{4}$$

We note in passing that the above propagation can be carried out entirely with real algebra, which results in significant savings over the complex time propagation.

The discretization of the Hamiltonian is the same as in our previous work[18,31] and thus not detailed here. Briefly, a direct product discrete variable representation (DVR) was employed.[56] Along the Jacobi radial coordinates R and r, equidistant grids were defined and the corresponding kinetic energy terms were evaluated using the fast sine Fourier transform. For the angular variable γ, Gauss–Legendre DVR points were used.

B. Bound-state calculations

In addition to the resonance calculations, we have included below some calculations of the highly excited bound states using the similar techniques as in our earlier work.[31,57] In particular, the bound states were obtained using the Lanczos method[58] and Radau coordinates. A single Lanczos propagation method[59,60] was used to identify the local mode[61] states by computing within a single Lanczos recursion all the overlaps between the eigenstates and several Gaussian wave packets strategically placed near the dissociation asymptotes.[57] The reader is referred to our earlier publications[31,57] for details.

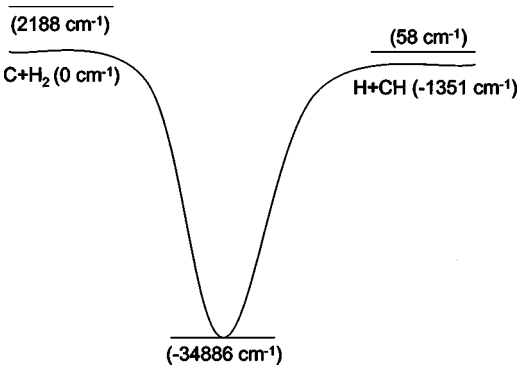

FIG. 1. Energetics of the $C(^1D)+H_2 \rightarrow CH+H$ reaction, including the zero-point energies in both arrangement channels. The energy zero is chosen at the potential minimum of the reactant $(C+H_2)$ channel.

C. Periodic orbit calculations

To understand the classical motion below and above the dissociation limit, we have performed periodic orbit (PO) analysis of the phase space structure. Stationary points and periodic orbits were located with the program POMULT, a package of Fortran programs which implement multiple shooting algorithms for solving two-point boundary value problems.[62] Analytic first and second derivatives of the potential function required in the calculation of periodic orbits and their stability analysis were computed by the AUTO_DERIV, a Fortran code for automatic differentiation of any analytic function of many variables written in Fortran.[63] Details can be found in our previous publications.

III. RESULTS AND DISCUSSION

A. General properties of resonances

Convergence tests have been carried out by varying the basis size along each degree of freedom in the resonance calculations. The numerical parameters finally employed are summarized as follows: 188 equidistant grid points for $R \in (0.0, 16.0)a_0$, 99 equidistant grid points for $r \in (0.5, 15.0)a_0$, and 35 Gauss–Legendre quadrature points for the angular coordinate, which correspond to $j_{\max}=68$ because of the exchange symmetry in the diatom. This large $(N=6.5\times10^5)$ dimensionality of the propagation wave packet is the same as in our earlier bound-state calculation.[31] The PES and the rotational kinetic energy terms were truncated at 0.5 hartree. The damping starts at $R_d=11.0a_0$ and $r=11.0a_0$ with damping coefficients of $5.0\times10^{-4}a_0^{-2}$ and $4.0\times10^{-3}a_0^{-2}$.

In Fig. 1, the energetics of the $C(^1D)+H_2 \rightarrow CH+H$ reaction including the zero point energy in each arrangement channel is illustrated. The bimolecular reaction is slightly exothermic. The product (CH+H) asymptotic limit is 58 cm^{-1} above the reference zero, which is chosen as the reactant $(C+H_2)$ PES minimum. The reactant channel opens at 2188 cm^{-1}. We should, however, caution that these threshold energies are not strictly defined as the PES is not perfectly flat in the asymptotic regions. There is an uncertainty of about 10 cm^{-1}.

In calculating the CH_2 resonance states, we have generated two sets of correlation functions using different initial wave packets ψ_i. The first was a doubled autocorrelation function, generated by propagating an initial wave packet randomly distributed in the coordinate space, while the second set included both autocorrelation and cross-correlation functions from a Gaussian initial wave packet in the $C(^1D)+H_2$ asymptote corresponding to the ground rovibrational state of $H_2(v_i=0, j_i=0)$. The former was aimed at a more statistically even sampling of resonance states, as the chosen initial wave packet has no inherent bias against any subset of resonances. On the other hand, the latter was used to identify resonances that play a major role in the reactive scattering, especially when cross-correlation functions involving the product channels $[C_k^{(f\leftarrow i)} \equiv (\psi_f|T_k|\psi_i)]$ were used in the LSFD analysis.

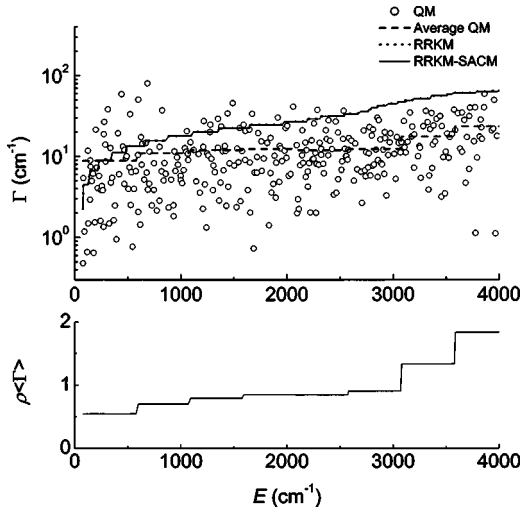

FIG. 2. Upper panel: resonance widths of the CH_2 system and the comparison of the averaged quantum rate $\langle k \rangle$ with the RRKM and SACM rates. Lower panel: the product of the density of state and average width of the resonances. The energies in abscissa are in reference to the potential minimum of the $C+H_2$ reactant valley.

A total of 320 resonance states were extracted in the energy range of $[0, 4000]$ cm^{-1} from the autocorrelation function with a random initial wave packet. The length of the correlation function is two hundred thousands, doubled from one hundred thousand propagation steps. Their energies and widths are displayed in the upper panel of Fig. 2 in open circles and those below 2000 cm^{-1} are listed in Table I. We emphasize at this point that the FD method is not designed for identifying broad $(\Gamma_n > 100$ $cm^{-1})$ resonances. The lack of resonances with widths larger than 20 ps^{-1} in Fig. 2 does not necessarily imply the absence of broad resonances.

As shown in Fig. 2, the width of the resonances fluctuates by more than two orders of magnitude, but no clear progression can be found. Similar to the highly excited bound-state spectrum,[31] the resonance states appear to be evenly spaced, presumably because of strong nearest neighbor level repulsion due to intermodal coupling. As expected,[64] the width on average becomes larger at higher energies and fluctuates less.

B. Phase space structure

We extracted the global classical dynamics of methylene on the $\tilde{a}\,^1A_1$ state PES by locating families of POs. We

TABLE I. Position and widths of CH_2 resonances below 2000 cm^{-1} in the units of cm^{-1}.

E	$\Gamma/2$	E	$\Gamma/2$	E	$\Gamma/2$	E	$\Gamma/2$
78.47	0.24E+00	490.80	0.50E+01	973.55	0.39E+01	1489.96	0.23E+02
81.93	0.27E+01	507.57	0.20E+01	999.87	0.29E+01	1504.42	0.38E+01
91.32	0.59E+00	517.83	0.37E+01	1000.10	0.25E+01	1525.26	0.12E+01
118.83	0.33E+00	522.84	0.17E+02	1013.90	0.23E+01	1532.56	0.62E+01
126.87	0.59E+01	527.71	0.13E+01	1028.41	0.34E+01	1544.89	0.42E+01
128.53	0.74E+00	535.71	0.32E+01	1039.63	0.63E+01	1555.32	0.11E+02
146.23	0.15E+01	545.60	0.38E+00	1050.48	0.57E+01	1563.85	0.14E+01
147.90	0.45E+01	559.59	0.20E+01	1059.03	0.10E+02	1578.27	0.58E+01
152.07	0.37E+01	577.42	0.33E+01	1067.55	0.54E+01	1592.93	0.12E+02
162.99	0.25E+01	599.02	0.52E+01	1070.49	0.45E+01	1607.49	0.45E+01
174.49	0.31E+01	599.78	0.10E+01	1092.85	0.75E+01	1609.63	0.10E+02
179.15	0.32E+00	600.70	0.25E+02	1122.53	0.60E+01	1632.39	0.19E+01
190.09	0.77E+00	617.31	0.72E+00	1145.90	0.24E+01	1648.09	0.11E+02
200.14	0.11E+02	625.89	0.87E+01	1168.13	0.53E+01	1651.90	0.42E+01
209.89	0.36E+01	632.46	0.39E+01	1180.47	0.18E+01	1654.09	0.10E+01
218.59	0.20E+01	639.12	0.72E+01	1209.12	0.11E+01	1673.69	0.17E+02
231.03	0.29E+01	655.64	0.26E+01	1212.71	0.66E+01	1686.29	0.36E+00
243.40	0.80E+00	671.99	0.73E+01	1217.80	0.14E+02	1695.90	0.32E+01
247.76	0.19E+01	679.49	0.31E+01	1228.00	0.22E+01	1717.47	0.32E+01
257.53	0.22E+01	687.57	0.40E+02	1241.50	0.66E+00	1718.47	0.49E+01
265.30	0.19E+01	690.11	0.19E+01	1249.01	0.54E+01	1729.65	0.97E+01
272.40	0.67E+00	703.43	0.23E+01	1259.43	0.51E+01	1760.57	0.77E+01
276.42	0.94E+01	706.53	0.57E+01	1276.74	0.10E+02	1763.60	0.33E+01
279.55	0.13E+02	728.34	0.12E+01	1280.42	0.12E+02	1782.92	0.47E+01
289.34	0.70E+01	747.70	0.19E+01	1289.84	0.47E+01	1813.94	0.73E+01
292.64	0.43E+01	749.00	0.41E+01	1304.42	0.19E+01	1831.03	0.70E+00
314.27	0.19E+02	775.19	0.11E+01	1308.76	0.39E+01	1845.64	0.31E+01
325.59	0.74E+00	799.45	0.14E+01	1322.00	0.32E+01	1847.18	0.84E+01
338.95	0.63E+01	800.61	0.66E+01	1350.79	0.64E+01	1855.16	0.18E+01
341.94	0.24E+01	819.94	0.33E+01	1352.25	0.15E+02	1873.38	0.23E+01
353.47	0.27E+01	825.06	0.19E+02	1361.78	0.14E+01	1884.54	0.51E+01
368.80	0.81E+00	839.21	0.25E+01	1376.32	0.24E+01	1896.20	0.15E+01
380.72	0.12E+01	847.92	0.41E+01	1383.89	0.12E+01	1900.07	0.42E+01
393.50	0.47E+00	859.28	0.30E+01	1397.44	0.58E+01	1915.54	0.15E+02
409.87	0.96E+01	886.13	0.12E+01	1403.32	0.34E+01	1927.94	0.24E+01
419.32	0.30E+01	910.28	0.26E+01	1415.73	0.67E+01	1934.13	0.67E+01
443.48	0.29E+02	931.62	0.12E+01	1422.81	0.58E+01	1941.07	0.63E+01
455.57	0.66E+01	932.44	0.91E+00	1429.88	0.12E+01	1955.43	0.44E+01
468.48	0.23E+01	940.98	0.58E+01	1443.32	0.17E+02	1978.28	0.59E+01
470.84	0.60E+01	950.13	0.33E+01	1447.54	0.21E+01	1988.67	0.11E+02
483.64	0.48E+01	967.25	0.48E+01	1460.78	0.41E+01	1996.32	0.48E+01

started from the minimum of the PES by finding the principal families which correspond to the normal modes of the molecule. Then, continuation methods applied with the time period as a parameter[65] revealed how the stability of the POs change with energy in a specific family. Bifurcations were predicted and new families of POs were located. The continuation/bifurcation (C/B) diagram was then compared with the quantum mechanical vibrational overtone level spacing. We have covered energies up to 5000 cm^{-1} above the dissociation threshold.

The C/B diagram is shown in Fig. 3. The continuous lines denote the frequencies of POs as functions of the total energy E. A3 is the family that corresponds to the bending normal mode, A2 to the symmetric stretching mode, and A1 to the antisymmetric stretching mode. The continuation lines do not distinguish stable from unstable POs. The A1 family remains stable for the energy range shown, but the A2 symmetric stretch family becomes early single unstable and after its bifurcation at about $-25\,400$ cm^{-1} double unstable. Note that the two principal families A1 and A2, cross at about $-12\,000$ cm^{-1} with A1 having lower frequencies than A2 at higher energies. The bifurcation of A2, the A2A1 family, shows larger anharmonicity than the parent A2 and it is initially single unstable but it becomes stable above $-20\,000$ cm^{-1} and remains stable up to the dissociation of the molecule. A3 is stable up to the barrier of isomerization that separates the two symmetric minima of the PES, after which it becomes single and later double unstable.

As shown in our previous studies,[66–69] the Hamiltonian saddle-node (SN) bifurcation is the most common elementary bifurcation[70] found in molecular systems. Their importance is due to the creation of new POs suddenly at some

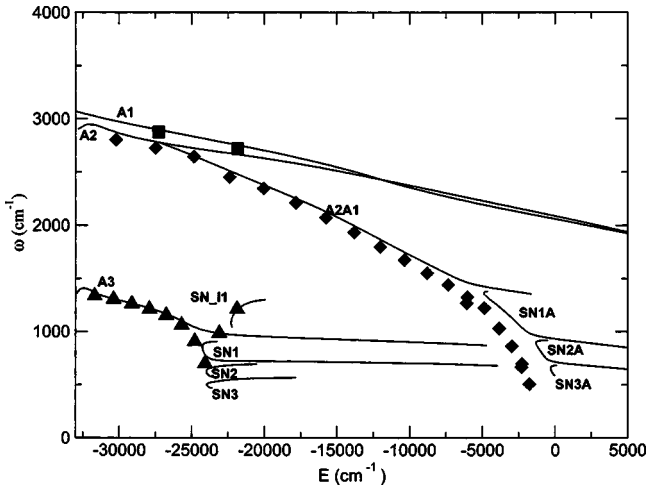

FIG. 3. Periodic orbit continuation/bifurcation diagram of the $\tilde{a}\,^1A_1$ state of CH_2. A3 is the family that corresponds to the bending normal mode, A2 to the symmetric stretching mode, and A1 to the antisymmetric stretching mode. The symbols represent the energy spacing between neighboring quantum states of the overtone progressions; squares for the antisymmetric stretch, diamonds for the symmetric stretch, and local mode and triangles for the bend. SN denotes periodic orbits emanated from saddle-node bifurcations. Note also that the even quantum number states for the antisymmetric stretch are shown.

critical energy with stable motions embedded in chaotic regions. That causes the localization of energy, a significant effect in chemical dynamics. Cascades of such SN bifurcations (SNi) appear as we approach the saddle point of the linearized molecule and the dissociation threshold, as shown in Fig. 3. This scenario, seen also previously, is typical as the parent family approaches the bifurcation critical energy. Its frequency levels off and two new families appear with one branch showing high anharmonicity. As energy increases the frequency of the most anharmonic daughter family starts leveling off again and a new SN bifurcation takes place.

The bifurcation of the A2 family, A2A1, results in local mode type motions (CH stretch), which continue even above the dissociation threshold. To understand these classical local mode dynamics, we have identified the quantum mechanical local mode overtones of CH_2 below the dissociation limit, denoted as the $(n,0)^+$ states,[61] using the method of Li and Guo.[57] As shown in Table II, the energy gap between adjacent levels decreases from $\sim$2800 cm^{-1} to merely 500 cm^{-1}, due to large anharmonicity in the dissociation channels. In Fig. 3, the classical frequencies are compared with the energy difference between adjacent quantum eigenenergies for the three series of overtone vibrational progressions. As we can see, the anharmonicity of the overtone states closely follows that of the frequencies of the POs.

Most importantly, the highly excited local mode eigenfunctions near the dissociation threshold seem to correspond to the saddle-node type POs:SNiA. A typical example is shown in Fig. 4, in which the $(14,0)^+$ eigenfunction at -3097.86 cm^{-1} is plotted in the Radau coordinates together with a PO from the SN1A family and its symmetric counterpart. The existence of stable POs, such as the A1 and A2A1 families, allows us to conclude that regularity exists in the largely chaotic phase space even above the dissociation limit.

TABLE II. Energies (in cm^{-1}) and assignments of local mode states below the dissociation limit. The underlined energies indicate that no unique assignment is possible due to mode mixing.

$E_n - E_0(-31\,249.39)$	Assignment
0.00	$(0,0)^+$
2 803.56	$(1,0)^+$
5 530.04	$(2,0)^+$
8 175.93	$(3,0)^+$
10 628.27	$(4,0)^+$
12 974.81	$(5,0)^+$
15 187.28	$(6,0)^+$
17 258.07	$(7,0)^+$
19 191.71	$(8,0)^+$
20 989.60	$(9,0)^+$
22 665.57	$(10,0)^+$
24 218.50	$(11,0)^+$
25 660.20	$(12,0)^+$
26 928.96	$(13,0)^+$
26 986.36	
28 151.53	$(14,0)^+$
29 180.62	$(15,0)^+$
30 043.98	$(16,0)^+$
30 742.80	$(17,0)^+$
30 711.16	
30 660.21	
31 249.80	$(18,0)^+$

C. Unimolecular decay rate

In the limit of isolated resonances, the unimolecular decay rate of a resonance is directly related to its width,[32]

$$k_n = \Gamma_n/\hbar, \tag{5}$$

where $\hbar$ is the Planck's constant. As shown in the lower panel of Fig. 2, the CH_2 resonances are mostly isolated below 3000 cm^{-1}, judging from the product of density of states and average width ($\rho\langle\Gamma\rangle$). Here, the density of states ρ was obtained directly from the resonance spectrum with a

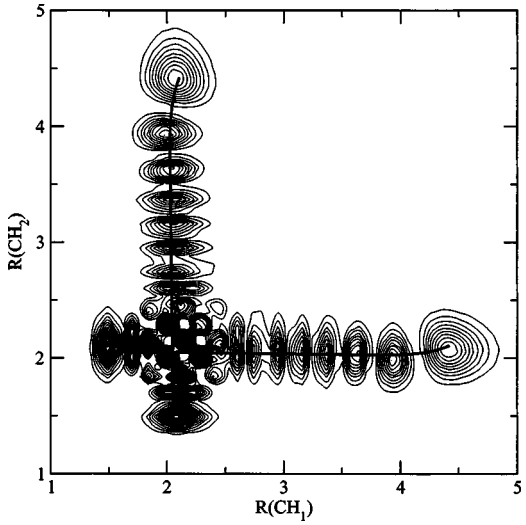

FIG. 4. Wave function of a local mode $[(14,0)^+]$ bound state marked by a periodic orbit of the SN1A family (see text) and its symmetric counterpart at approximately the same energy. The Radau coordinates are used with the Radau angle fixed at 92.22°.

500 cm^{-1} interval. However, it was found to be very close to that extrapolated from the bound-state spectrum, which gave us some confidence that most resonances have been captured by our calculation. Above 3000 cm^{-1}, the density of states is larger than the average width and the resonances are likely to overlap. In this limit, the decay rate is more difficult to define. In addition, the opening of the $C+H_2$ channel at 2188 cm^{-1} is expected to complicate the decay dynamics. For these reasons, we will concentrate in this section on the lowest-lying resonances up to 2000 cm^{-1}. In our discussion, k_n and Γ_n will be used interchangeably.

The two archetypes of unimolecular decay are the so-called statistical state-specific and mode-specific limits,[32,64,71,72] exemplified by the HO_2 (Refs. 73 and 74) and HCO systems,[75,76] respectively. The former is characterized by complicated and irregular vibrational wave functions due to strong intermodal coupling and random energy distribution among the internal degrees of freedom. As a result, the corresponding resonance states cannot be assigned with a zeroth-order Hamiltonian. On the other hand, the latter exhibits strong dependence of the decay rate on one or more regular and assignable vibrational progressions, thanks to weak coupling of these modes with the dissociation coordinate. Naturally, wave functions of these resonances show clear nodal structures and are assignable based on a zeroth-order Hamiltonian. A direct result of mode specificity is a large fluctuation of the resonance width. In HCO,[76] for instance, resonance widths span more than four orders of magnitude and depend sensitively on the vibrational assignment. However, statistical state-specific decay processes do not necessarily possess uniform widths either, unless in the limit of infinite decay channels. Indeed, resonance widths of the HO_2 system also fluctuate, but within a smaller range.[74] It is interesting to note that the fluctuation of the width in the statistical limit is well characterized by the Porter–Thomas distribution[77,78] that can be derived from the random matrix theory[79] or from maximal entropy arguments.[80]

The CH_2 system is certainly not a regular system, as shown by our earlier analysis of its vibrational spectrum below the dissociation limit,[31] in which many highly excited vibrational states were found to be irregular and unassignable. Intermodal couplings, such as the Fermi resonance between the stretching and bending modes, and anharmonicities are responsible for strong mode mixing and random energy distribution among the internal modes.

If the decay of CH_2 is not mode specific, is it statistical state specific? The quantum state specificity is well illustrated in Fig. 2, where decay rates of low-lying resonances are scattered over more than two orders of magnitude. To examine whether the decay is statistical, we compared the resonance widths with the Rice–Rampsberger–Kassel–Marcus (RRKM) rate for given E and J,[32]

$$\Gamma^{\mathrm{RRKM}}(E) = \frac{N(E)}{2\pi\hbar\rho(E)}, \tag{6}$$

where $\rho(E)$ is the density of states at E and $N(E)$ is the total number of open channels at the transition state. The RRKM theory is based on the premise that the system is completely ergodic because of fast intramolecular vibrational energy redistribution. As a result, it yields decay rates for the limiting case of a completely statistical unimolecular reaction. Technically, there are several ways to compute the numerator in Eq. (6). As an upper limit, it can be approximated by the number of asymptotic open channels at a given energy for a barrierless system such as CH_2. Alternatively, the statistical adiabatic channel model (SACM),[81] in which the number of open channels is counted based on adiabatic dissociation potential curves, can be used. To that end, we have computed the adiabatic eigenvalues of the two-dimensional Hamiltonian matrices along the dissociation coordinate and constructed the adiabatic curves for both the CH+H and C $+H_2$ channels. In the energy range below 4000 cm^{-1}, the results from the two modals are nearly identical, thanks to very "loose" transition states in both arrangement channels.

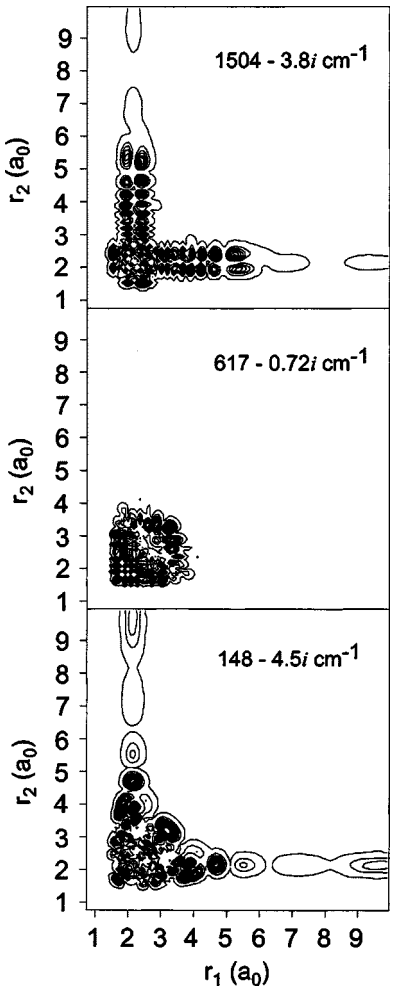

FIG. 5. Contour plots of representative local mode (upper panel), hyperspherical mode (middle panel), and irregular (lower panel) resonance wave functions. These wave functions in the internal [$r_i = r(C-H_i)$, $i=1,2$ and θ being the enclosed angle] coordinates are interpolated from the reactant Jacobi coordinates. The angle is fixed at 80°, 100°, and 100° for the three figures, respectively.

The rates predicted by the RRKM and SACM models are compared in Fig. 2 with the averaged quantum rate $\langle k \rangle$ of CH_2. Here, $\langle k \rangle$ was calculated as an arithmetic average of the rate within a small (500 cm^{-1}) energy interval. The comparison clearly shows that the statistical models overestimate the averaged decay rate by roughly a factor of 2. It implies that

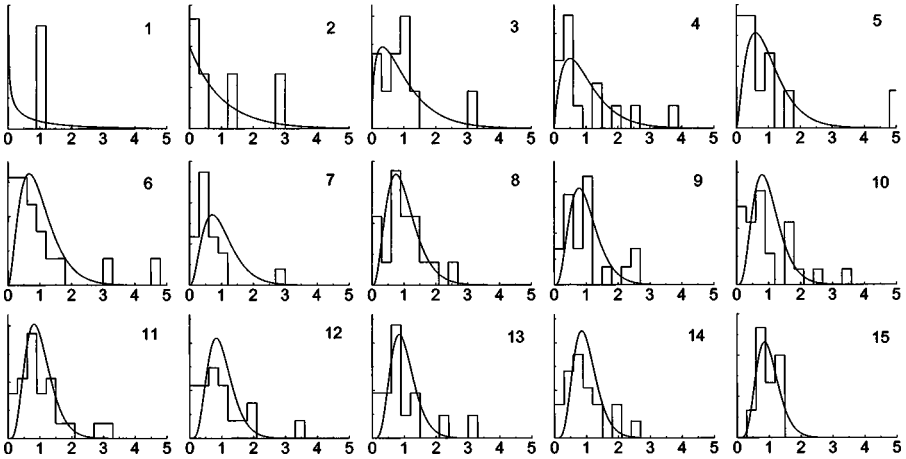

FIG. 6. Comparison of the distribution of the resonance decay rates (histogram) and the Porter–Thomas distribution (line) for different N. Each box corresponds to the distribution in the energy interval $[E(N),E(N+1)]$ where N enumerates the open channel. The x axis is $k/\langle k\rangle$ and the area of the distribution is all normalized to unity.

the decay of the CH_2 complex might not be completely statistical. This observation is consistent with our analysis of the CH_2 vibrational spectrum near the dissociation limit (Sec. III B and Ref. 31), in which regularity was found embedded in the chaotic classical phase space. Indeed, a Brody parameter of 0.64 was found for the nearest neighbor level spacing distribution of the CH_2 vibrational spectrum,[31] where 0 and 1 are known for regular (Poisson) and irregular (Wigner) limits, respectively.[82] Significant deviations from the irregular Gaussian orthogonal ensemble limit were also observed in the Δ_3 distribution.

The regularity stems, at least partly, from the local mode[61] stretching vibration of CH_2. As discussed in Sec. III B, many local mode states have been found below the dissociation limit and the local mode POs are stable even above the dissociation threshold. We have also found many resonance states possess clear local mode characteristics. As shown in the upper panel of Fig. 5, the wave function of one of such states ($E_n=1540\ \mathrm{cm}^{-1}$) extends in the two dissociation coordinates with a clear nodal structure. Similar local mode states have previously been observed below and above the dissociation limit of H_2O on model[83,84] and realistic potential energy surfaces.[57,85] Because of their extended wave functions in the dissociation channels, they often have relatively short lifetimes. For the local mode resonance state shown in Fig. 5, its width of 7.6 cm^{-1} is significantly larger than the average width in this energy range.

In contrast to the local mode vibration where energy is stored in one of two C–H stretching modes, excitation can also be shared by both stretching modes to form the so-called hyperspherical mode.[83–85] We have found resonance states that resemble hyperspherical mode of vibration, and plotted in the middle panel of Fig. 5 one such wave function ($E_n=617\ \mathrm{cm}^{-1}, \Gamma_n=1.4\ \mathrm{cm}^{-1}$). Because of the compactness of wave functions, such resonances typically have smaller overlaps with continuum states and thus on average longer lifetimes. Nonetheless, the nodal structure is clear and assignable.

The presence of both the local and hyperspherical modes in the CH_2 resonance states points to many similarities with the more extensively studied H_2O system,[83–85] presumably because of similar mass disparities in these systems. Both vibrational spectra are largely chaotic, but with surviving regularities to the dissociation limit and beyond. Indeed, such similarities have been noted by other authors.[86]

The local and hyperspherical states notwithstanding, the majority of the CH_2 resonances are irregular and impossible to assign quantum numbers based on any zeroth-order Hamiltonian. A representative state at $E_n=148\ \mathrm{cm}^{-1}$, $\Gamma_n=9.0\ \mathrm{cm}^{-1}$ is plotted in the lower panel of Fig. 5. The lack of clear nodal structure is a result of strong intermodal coupling that facilitates efficient energy flow among the vibrational modes. However, because only a finite number of dissociation channels is available at low energies in this small polyatomic system, the width of the resonances fluctuates. As mentioned earlier, the fluctuation of the resonance width should in the statistical limit follow the so-called Porter–Thomas distribution,[77–80]

$$P(k)=\frac{N}{2\langle k\rangle}\left(\frac{Nk}{2\langle k\rangle}\right)^{(N-2)/2}\frac{\exp(-Nk/2\langle k\rangle)}{\Gamma(\mathrm{N}/2)}, \tag{7}$$

where $\langle k\rangle$ is the average rate within an energy interval $[E,E+dE]$, N is the effective number of open channels, and $\Gamma(x)$ is the Gamma function. In Fig. 6, the distribution of the resonance decay rates is compared with the Porter–Thomas distribution for the first 15 open channels. Due to the small number of resonance states in each energy window, particularly those at low energies, the binned distributions may not be smooth and statistical. However, the agreement with the Porter–Thomas distribution is reasonable, although there appears to have some overpopulation of resonances with extremely small rates. In particular, we note that the range of fluctuation decreases with the energy while the averaged width increases with the energy. With an increasing number of open channels, the Porter–Thomas distribution eventually approaches the δ-function limit centered at the average rate $\langle k\rangle$, where the RRKM theory is expected to give an accurate description of the unimolecular decay.[32]

To summarize, the unimolecular decay of the CH_2 sys-

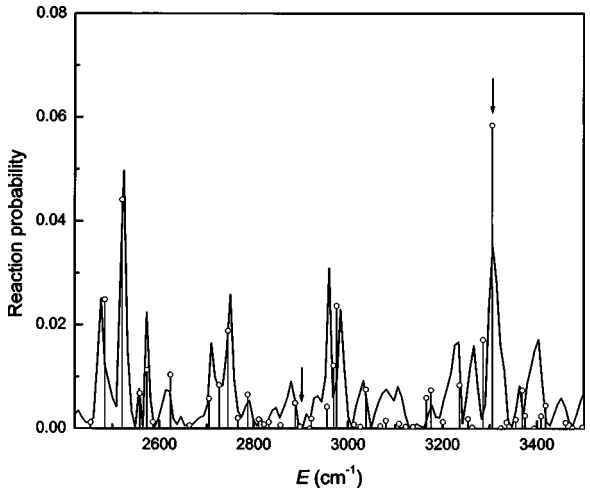

FIG. 7. Reaction probability for the $v_f=0, j_f=0 \leftarrow v_i=0, j_i=0$ transition (line) and the contribution of the narrow ($\Gamma \leqslant 25$ cm^{-1}) resonances (circles). The product of the overlaps of the resonance with the initial and final wave packets [see Eq. (8)] is shown in the figure as the height of each resonance.

tem into the CH+H channels is neither mode specific nor statistical state selective. Rather, it is an intermediate case between the two limits. Like in its bound-state spectrum, the low-lying resonances of CH_2 possess significant regularity embedded in the largely chaotic classical phase space in the form of local and hyperspherical modes. Similar observations have been made for other systems such as HNO (Ref. 71) and C_2H.[87,88]

D. Bimolecular reaction

Below 2188 cm^{-1}, the resonances can only decay into the product (CH+H) channels and do not contribute to the bimolecular reaction. Above 2188 cm^{-1}, resonances can decay into the reactant or product channels or both. As a result, the resonances that affect the bimolecular reaction are expected to be quite different from those responsible for the unimolecular reaction discussed above.

As mentioned in Sec. II, resonances have also been extracted from the correlation functions associated with an initial wave packet in the reactant ($C+H_2$) channel. Many of them are identical to those extracted from the autocorrelation function with the random initial wave packet, but others converge better because of larger overlaps with the initial wave packet in the reactant channel. In Fig. 7, the resonances are plotted with the state-to-state reaction probability ($P_{v_f=0,j_f=0\leftarrow v_i=0,j_i=0}$) in the energy range $[2420, 3500]$ cm^{-1}. The reaction probability is expressed as the square of the corresponding S-matrix element ($|S_{v_f=0,j_f=0\leftarrow v_i=0,j_i=0}|^2$), which is obtained by Fourier transform of the cross-correlation function $C_k^{(f\leftarrow i)}$, see Ref. 20 for details.

To shed light on the comparison, we express the S-matrix element in terms of contributions of individual resonances $|n)$,[89,90]

$$S_{f\leftarrow i}(E) = \frac{i(\psi_f|G^+(\hat{H}-E)|\psi_i)}{2\pi a_i(E)a_f^*(E)} = \frac{i}{2\pi a_i(E)a_f^*(E)}\sum_n \frac{(\psi_f|n)(n|\psi_i)}{E-E_n+i\Gamma_n/2}, \quad (8)$$

where a_i and a_f are amplitudes of the initial and final wave packets at energy E, respectively. We emphasize that the resonance states have to be complete to span the Green's operator in Eq. (8). If the resonances are isolated, each resonance contributes to a Lorentzian peak in the reaction probability, whose intensity is proportional to the square of its overlaps with both the initial and final wave packets ($|(\psi_f|n)(n|\psi_i)|^2$). Indeed, such correspondence can be observed at the low energy end of the spectrum in Fig. 7, where the square of each resonance contribution is plotted as the height of the resonance. Although the peak positions do not coincide perfectly with the resonance energies, each peak in the reaction probability can still be attributed to a single resonance.

However, we have shown in Fig. 2 that the resonance widths are on average larger than the nearest neighbor level spacing in this energy range. In this overlapping resonance limit, the decomposition of the peaks into contributions of individual resonances becomes much more difficult because of quantum interferences with many nearby resonances, particularly those with large widths. Note that the reaction probability is the square of a coherent sum of all resonance contributions. These interferences may shift peak positions, produce new peaks, or alter the peak intensities. Perhaps more importantly, the list of resonances may miss many states with very large widths. The interference of these very broad resonances with the narrow resonances shown in the figure is very difficult to estimate. Thus, a faithful reconstruction of the reaction probability from the narrow resonances is understandably difficult, if not impossible, to achieve.

Even though the peaks in the reaction probability cannot be directly assigned to individual resonances, there is little doubt that the oscillatory structures in the state-to-state and total reaction probabilities are due to either the resonances themselves or their interferences. Thus, it is instructive to examine individual resonances that contribute to the bimolecular reaction. The upper panel of Fig. 8 shows a representative wave function of a resonance state at $E=3306-20i$ cm^{-1}. As indicated in Fig. 7 by an arrow, it has a significant overlap with both the initial and final wave packets. Typically, the resonances that affect the bimolecular reaction possess significant amplitude in both the reactant ($C+H_2$) and product (CH+H) channels, whereas those dominating the unimolecular reaction have their energy stored in the C–H vibration, as shown in Fig. 5. To illustrate the difference between these two types of resonances, we plot in the lower panel of the same figure the wave function of another resonance ($E=2898-4i$ cm^{-1}) that has a very small amplitude in the reactant channel. Its negligible contribution to the bimolecular reaction is highlighted by another arrow in Fig. 7.

Finally, we note from the upper panel of Fig. 2 that the

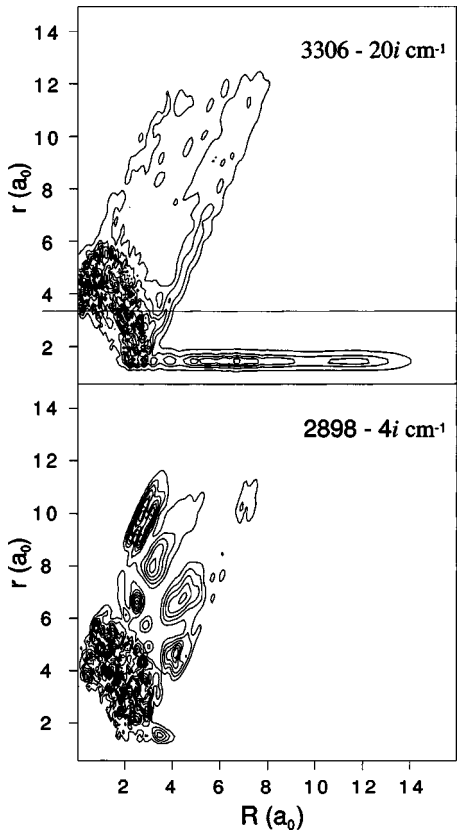

FIG. 8. Contour plots of two representative resonance states in the reactant Jacobi coordinates as $|\psi(R,r)|^2$ with the angular degree of freedom integrated out.

resonance lifetimes are typically on the order of a picosecond. A significant portion of the low-lying resonances has lifetimes comparable to the rotational period of the molecule. The overlapping of resonances in the energy range of interest may further enhance the energy randomization in the excited CH_2 complex, rendering the system more statistical. These observations justify the assumptions used in the statistical treatment of the $C(^1D)+H_2$ reaction,[21–24] i.e., the sufficiently long lifetime of the CH_2 complex permits the neglect of phase information in computing reaction probabilities of the bimolecular reaction.[91,92]

IV. CONCLUSIONS

In this work, we have studied low-lying resonances of the CH_2 system on a high quality *ab initio* potential energy surface using the low-storage filter-diagonalization method based on the Chebyshev propagation, and examined their roles in both unimolecular and bimolecular reactions. A few hundred narrow resonances were found in the energy range up to $\approx$4000 cm^{-1} above the lowest dissociation asymptote. They exhibit a large variation in their widths, suggesting strong state specificity. On average, the resonance width increases with energy, but its fluctuation decreases. While the resonances are mostly isolated at lowest energies, they become increasingly overlapped as energy increases.

These metastable resonances can be considered as an extension of the highly excited vibrational states beyond the dissociation limit. Hence, they have properties that resemble those of the bound states. Indeed, our analysis of the classical phase space indicates that many periodic orbits extend smoothly into the continuum. This observation implies that a good understanding of the resonances can be achieved by studying the highly excited vibrational levels.

Below 2000 cm^{-1} where the resonances are mostly isolated, the unimolecular decay into the CH+H channels is dominated by individual CH_2 resonances. The decay of these resonances is found to conform to neither the mode-specific nor statistical state-specific limits. This is consistent with our understanding of the vibrational dynamics near the dissociation limit, which shows regularity embedded in the largely chaotic classical phase space. Indeed, the fluctuation of the resonance width is reasonably well described by the Porter–Thomas distribution derived from the random matrix theory. However, significant regularity persists in both highly excited bound states and low-lying resonances. In particular, we have found resonances possessing clear nodal structures related to local and hyperspherical vibrational modes. Furthermore, classical analysis of the phase space has identified many saddle-node periodic orbits, which can be regarded as the classical analogs of the regular quantum resonance states. Because of these regular resonances, statistical theories such as the RRKM and SACM models overestimate the averaged quantum decay rate in this energy range. The coexistence of regular and irregular resonances states makes the CH_2 system an intermediate case between the two limiting cases of unimolecular reactions.

Like other XH_2 hydrides such as water, the CH_2 system presents an interesting case for studying mode-selective chemistry and intramolecular vibrational energy redistribution. Kinematic factors such as the mass disparity between H and *X* favor the existence of local modes, which in turn suggests the possibility of selectively exciting one of the two C–H bonds. For an isotopomer CHD, for example, mode-selective excitation might lead to preferential branching of the products, namely, CD and CH. It is interesting to note that this system differs from completely regular systems such as HCO in that the mode-selective unimolecular reaction is embedded in a largely chaotic classical phase space. We hope that the results in this work will motivate future experimental exploration of the unimolecular decay of CH_2, even though specific prediction of resonance energies and widths made in this work may not be quantitatively accurate.

The bimolecular reaction is also dominated by resonances. Our results unequivocally confirm that the oscillation structure observed in bimolecular reaction probabilities is due to resonances, many of them are long lived and overlap with each other. As a result, it is difficult to assign the peaks in the reaction probability to individual resonance states. However, the lifetimes of many resonances are sufficiently long to permit a statistical treatment of the bimolecular reaction, as illustrated in recent work by us and others.

Resonances affecting the bimolecular reaction exhibit very different characteristics from those that dominate the unimolecular reaction. The former are found to have significant amplitudes in both the reactant and product channels, whereas the latter deposit their energy mainly in the C–H vibration. The detailed analysis presented in this work allows

us to gain deeper insight into the roles played by the long-lived resonances in both the unimolecular and bimolecular reactions.

ACKNOWLEDGMENTS

The work at UNM was supported by the National Science Foundation (Grant No. CHE-0348858), and funding at UC was provided by the Greek Ministry of Education and European Union through the postgraduate program EPEAEK, "Applied Molecular Spectroscopy." The authors thank Professor Bill Hase for stimulating discussions and Professor Reinhard Schinke for sending them his work prior to publication.

[1]A. G. Gaydon, *The Spectroscopy of Flames* (Chapman and Hall, London, 1974).
[2]D. R. Flower and G. Pineau des Forets, Mon. Not. R. Astron. Soc. **297**, 1182 (1998).
[3]P. Casavecchia, Rep. Prog. Phys. **63**, 355 (2000).
[4]K. Liu, Annu. Rev. Phys. Chem. **52**, 139 (2001).
[5]B. Bussery-Honvault, P. Honvault, and J.-M. Launay, J. Chem. Phys. **115**, 10701 (2001).
[6]T.-S. Ho, T. Hollebeek, H. Rabitz, L. B. Harding, and G. C. Schatz, J. Chem. Phys. **105**, 10472 (1996).
[7]K. Drukker and G. C. Schatz, J. Chem. Phys. **111**, 2451 (1999).
[8]S. K. Gray, C. Petrongolo, K. Drukker, and G. C. Schatz, J. Phys. Chem. **103**, 9448 (1999).
[9]R. A. Bearda, M. C. van Hemert, and E. F. van Dishoeck, J. Chem. Phys. **97**, 8240 (1992).
[10]G. M. Jursich and J. R. Wiesenfeld, J. Chem. Phys. **83**, 910 (1985).
[11]W. H. Fisher, T. Carrington, C. M. Sadowski, and C. H. Dugan, Chem. Phys. **97**, 433 (1985).
[12]D. C. Scott, J. deJuan, D. C. Robie, D. Schwartz-Lavi, and H. Reisler, J. Phys. Chem. **96**, 2509 (1992).
[13]K. Mikulecky and K.-H. Gericke, J. Chem. Phys. **98**, 1244 (1993).
[14]K. Sato, N. Ishida, T. Kurakata, A. Iwasaki, and S. Tsuneyuki, Chem. Phys. Lett. **237**, 195 (1998).
[15]A. Bergeat, L. Cartechini, N. Balucani *et al.*, Chem. Phys. Lett. **327**, 197 (2000).
[16]N. Balucani, G. Capozza, L. Cartechini *et al.*, Phys. Chem. Chem. Phys., **6**, 4957 (2004).
[17]L. Banares, F. J. Aoiz, P. Honvault, B. Bussery-Honvault, and J.-M. Launay, J. Chem. Phys. **118**, 565 (2003).
[18]S. Y. Lin and H. Guo, J. Chem. Phys. **119**, 11602 (2003).
[19]S. Y. Lin and H. Guo, J. Phys. Chem. A **108**, 2141 (2004).
[20]S. Y. Lin and H. Guo, J. Chem. Phys. **121**, 1285 (2004).
[21]E. J. Rackham, F. Huarte-Larranaga, and D. E. Manolopoulos, Chem. Phys. Lett. **343**, 356 (2001).
[22]E. J. Rackham, T. Gonzalez-Lezana, and D. E. Manolopoulos, J. Chem. Phys. **119**, 12895 (2003).
[23]S. Y. Lin and H. Guo, J. Chem. Phys. **120**, 9907 (2004).
[24]S. Y. Lin and H. Guo, J. Phys. Chem. A **108**, 10060 (2004).
[25]L. Banares, F. J. Aoiz, S. A. Vazquez, T.-S. Ho, and H. Rabitz, Chem. Phys. Lett. **374**, 243 (2003).
[26]R. J. Blint and M. D. Newton, Chem. Phys. Lett. **32**, 178 (1975).
[27]P. A. Whitlock, J. T. Muckerman, and P. M. Kroger, in *Potential Energy Surfaces and Dynamical Calculations*, edited by D. G. Truhlar (Plenum, New York, 1981).
[28]H. Petek, D. J. Nesbitt, D. C. Darwin, and C. B. Moore, J. Chem. Phys. **86**, 1172 (1987).
[29]G. V. Hartland, D. Qin, and H.-L. Dai, J. Chem. Phys. **102**, 6641 (1995).
[30]K. Kobayashi, L. D. Pride, and T. J. Sears, J. Phys. Chem. A **104**, 10119 (2000).
[31]S. C. Farantos, S. Y. Lin, and H. Guo, Chem. Phys. Lett. **399**, 260 (2004).
[32]T. Baer and W. L. Hase, *Unimolecular Reaction Dynamics, Theory and Experiments* (Oxford University Press, New York, 1996).
[33]L. D. Landau and E. M. Lifshitz, *Quantum Mechanics* (Pergamon, Oxford, 1977).
[34]G. Jolicard and E. J. Austin, Chem. Phys. **103**, 295 (1986).
[35]T. Seideman and W. H. Miller, J. Chem. Phys. **96**, 4412 (1992).
[36]D. Neuhauser, J. Chem. Phys. **93**, 2611 (1990).
[37]Y. Huang, D. J. Kouri, and D. K. Hoffman, Chem. Phys. Lett. **225**, 37 (1994).
[38]W. Zhu, Y. Huang, D. J. Kouri, C. Chandler, and D. K. Hoffman, Chem. Phys. Lett. **217**, 73 (1994).
[39]V. A. Mandelshtam and H. S. Taylor, J. Chem. Phys. **103**, 2903 (1995).
[40]V. A. Mandelshtam and H. S. Taylor, J. Chem. Phys. **102**, 7390 (1995).
[41]R. Chen and H. Guo, J. Chem. Phys. **105**, 1311 (1996).
[42]S. K. Gray and G. G. Balint-Kurti, J. Chem. Phys. **108**, 950 (1998).
[43]R. Chen and H. Guo, J. Chem. Phys. **105**, 3569 (1996).
[44]M. R. Wall and D. Neuhauser, J. Chem. Phys. **102**, 8011 (1995).
[45]V. A. Mandelshtam and H. S. Taylor, J. Chem. Phys. **106**, 5085 (1997).
[46]V. A. Mandelshtam and H. S. Taylor, J. Chem. Phys. **107**, 6756 (1997).
[47]R. Chen and H. Guo, Chem. Phys. Lett. **279**, 252 (1997).
[48]V. A. Mandelshtam and H. S. Taylor, Phys. Rev. Lett. **78**, 3274 (1997).
[49]V. A. Mandelshtam and H. S. Taylor, J. Chem. Soc., Faraday Trans. **93**, 847 (1997).
[50]D. Xie, R. Chen, and H. Guo, J. Chem. Phys. **112**, 5263 (2000).
[51]G. Li and H. Guo, Chem. Phys. Lett. **336**, 143 (2001).
[52]G. Li and H. Guo, Chem. Phys. Lett. **347**, 443 (2001).
[53]A. Neumaier and V. A. Mandelshtam, Phys. Rev. Lett. **86**, 5031 (2001).
[54]N. Moiseyev, P. R. Certain, and F. Weinhild, Mol. Phys. **36**, 1613 (1978).
[55]H. Tal-Ezer and R. Kosloff, J. Chem. Phys. **81**, 3967 (1984).
[56]J. C. Light and T. Carrington, Adv. Chem. Phys. **114**, 263 (2000).
[57]G. Li and H. Guo, J. Mol. Spectrosc. **210**, 90 (2001).
[58]C. Lanczos, J. Res. Natl. Bur. Stand. **45**, 255 (1950).
[59]R. Chen and H. Guo, J. Chem. Phys. **111**, 9944 (1999).
[60]R. Chen and H. Guo, J. Chem. Phys. **114**, 1467 (2001).
[61]M. S. Child and L. Halonen, Adv. Chem. Phys. **57**, 1 (1984).
[62]S. C. Farantos, Comput. Phys. Commun. **130**, 267 (2005).
[63]S. Stamatiadis, R. Prosmiti, and S. C. Farantos, Comput. Phys. Commun. **127**, 343 (2000).
[64]W. L. Hase, S.-W. Cho, D.-H. Lu, and K. N. Swamy, Chem. Phys. **139**, 1 (1989).
[65]E. L. Allgower and K. Georg, *Numerical Continuation Methods, Springer Series in Computational Mathematics*, Vol. 13, edited by R. L. Graham, J. Stoer, and R. Varga (Springer, Berlin, 1993).
[66]S. C. Farantos, Int. Rev. Phys. Chem. **15**, 345 (1996).
[67]H. Ishikawa, R. W. Field, S. C. Farantos, M. Joyeux, J. Koput, C. Beck, and R. Schinke, Annu. Rev. Phys. Chem. **50**, 443 (1999).
[68]M. Joyeux, S. C. Farantos, and R. Schinke, J. Phys. Chem. **106**, 5407 (2002).
[69]M. Joyeux, S. Y. Grebenshchikov, J. Bredenbeck, R. Schinke, and S. C. Farantos, Adv. Chem. Phys. (in press).
[70]S. Wiggins, *Introduction to Applied Nonlinear Dynamical Systems and Chaos* (Springer, New York, 2003).
[71]M. Stumpf, A. J. Dobbyn, D. H. Mordaunt, H.-M. Keller, H. Fluethmann, R. Schinke, H.-J. Werner, and K. Yamashita, Faraday Discuss. **102**, 193 (1995).
[72]S. Y. Grebenshchikov, R. Schinke, and W. L. Hase, *State-specific Dynamics of Unimolecular Dissociation* (Elsevier, Amsterdam, 2003).
[73]V. A. Mandelshtam, T. P. Grozdanov, and H. S. Taylor, J. Chem. Phys. **103**, 10074 (1995).
[74]A. Dobbyn, M. Stumpf, H.-M. Keller, and R. Schinke, J. Chem. Phys. **104**, 8357 (1996).
[75]D. Wang and J. M. Bowman, J. Chem. Phys. **100**, 1021 (1994).
[76]H.-M. Keller, H. Floethmann, A. J. Dobbyn, R. Schinke, H.-J. Werner, C. Bauer, and P. Rosmus, J. Chem. Phys. **105**, 4983 (1996).
[77]C. E. Porter and R. G. Thomas, Phys. Rev. **104**, 483 (1956).
[78]W. F. Polik, D. R. Guyer, W. H. Miller, and C. B. Moore, J. Chem. Phys. **92**, 3471 (1990).
[79]W. F. Polik, C. B. Moore, and W. H. Miller, J. Chem. Phys. **89**, 3584 (1988).
[80]R. D. Levine, Adv. Chem. Phys. **70**, 53 (1987).
[81]M. Quack and J. Troe, Ber. Bunsenges. Phys. Chem. **78**, 240 (1974).
[82]T. A. Brody, J. Flores, J. B. French, P. A. Mello, A. Pandey, and S. S. M. Wong, Rev. Mod. Phys. **53**, 385 (1981).
[83]B. Hartke, J. Manz, and J. Mathis, Chem. Phys. **139**, 123 (1989).
[84]B. Hartke, A. E. Janza, W. Karrlein, J. Manz, V. Mohan, and H.-J. Schreier, J. Chem. Phys. **96**, 3569 (1992).

[85]S. K. Gray and E. M. Goldfield, J. Phys. Chem. **105**, 2634 (2001).
[86]T. Joseph, J. Manz, V. Mohan, and H.-J. Schreier, Ber. Bunsenges. Phys. Chem. **92**, 397 (1988).
[87]R. J. Wolf and W. L. Hase, J. Chem. Phys. **72**, 316 (1980).
[88]R. J. Wolf and W. L. Hase, J. Chem. Phys. **73**, 3779 (1980).
[89]D. J. Kouri, Y. Huang, W. Zhu, and D. K. Hoffman, J. Chem. Phys. **100**, 3662 (1994).
[90]D. J. Tannor and D. E. Weeks, J. Chem. Phys. **98**, 3884 (1993).
[91]P. Pechukas and J. C. Light, J. Chem. Phys. **42**, 3281 (1965).
[92]W. H. Miller, J. Chem. Phys. **52**, 543 (1970).